Citric Acid and Epichlorohydrin as Crosslinking Agent on Hydrogel-Based Nanocellulose from Pine Cone Flower Potential for Wound Dressing Application

Masruri Masruri^{1*}, 'Urfa Zakiyya 'Uyunin¹, Muchammad Zainul Anwar¹, and Nur Ikhtiarini²

¹Department of Chemistry, Faculty of Mathematics and Natural Sciences, Brawijaya University, Jl. Veteran, Malang 65145, Indonesia

²Department of Chemical Engineering, Faculty of Engineering, UPN "Veteran" Jawa Timur, Jl. Raya Rungkut Madya, Gunung Anyar, Surabaya 60294, Indonesia

* Corresponding author:

email: masruri@ub.ac.id

Received: March 21, 2025 Accepted: July 8, 2025

DOI: 10.22146/ijc.105566

Abstract: Chronic wounds and bacterial infections require wound dressings with both moisture retention and antibacterial properties. This study developed a hydrogel from pine flower-derived nanocellulose crosslinked with citric acid (CA) and epichlorohydrin (ECH). Nanocellulose was characterized using TEM and PSA, confirming a size of 10–30 nm. Hydrogels were synthesized using CA and ECH as crosslinkers, and characterized via FTIR (chemical bonding), SEM (morphology), swelling tests, antibacterial assays, and UV-vis-based release studies. FTIR data confirmed successful crosslinking. SEM results revealed a porous structure ideal for wound healing; hydrogels without extract showed smoother surfaces than those with extract. ECH-crosslinked hydrogels exhibited higher swelling capacity, suitable for heavily exuding wounds. Hydrogels incorporating white dragon fruit peel extract demonstrated enhanced antibacterial activity against Staphylococcus aureus. Release studies showed controlled diffusion of active compounds, particularly in CA-crosslinked hydrogels. These findings suggest nanocellulose-based hydrogels with natural crosslinkers and plant extracts offer promising properties for wound dressing applications, combining moisture management with antibacterial functionality.

Keywords: hydrogel; nanocellulose; cross-linking; epichlorohydrin; citric acid

■ INTRODUCTION

Wound dressing is of utmost importance in the treatment of injuries and wound healing. It has a variety of functions, such as infection protection, creation of a moist microenvironment suitable for tissue repair, and exudate absorption preventing maceration of the adjacent skin [1]. Over the years, advancements in wound care have led to the development of a wide variety of dressing materials, ranging from traditional gauze and bandages to more advanced options such as hydrocolloids [2-4], hydrogels [5-6], bioactive dressings [7-8], and combinations [9]. The choice of a suitable wound dressing is influenced by various factors such as the nature, size, depth and degree of wound, but also by the condition of the patient in general [10]. Through the creation of the best healing environment, wound dressings play an important role in decreasing time to recovery and patient

satisfaction.

Materials for wound dressings used in previous studies have been shown to require the selection of biocompatible and functional materials to facilitate optimal healing. As these are inexpensive and readily available, traditional materials (e.g., cotton gauze and bandages) have been extensively employed. Yet, they are commonly derived from features that lack sophisticated functions, such as moisture retention and antimicrobial activity, but also primarily originated in organic engineering and chemistry. Recent studies have concentrated on the design of novel wound dressing materials based on natural polymers, such as cellulose [11], chitosan [12], alginate [13], known to be biodegradable, biocompatible, and to promote tissue regeneration. Furthermore, synthetic polymers including polyurethane and polyethylene glycol are investigated

due to their softness, strength and customizable properties [14-17]. Other high-potential technologies such as nanofiber scaffolds and hydrogel-based dressings have been shown to provide a moist environment, deliver drugs and protect against infections [17]. These developments emphasize the ongoing work to design wound dressings suitable for different wound states to promote healing without delay and with greater efficiency.

Hydrogel-based cellulose wound dressings have become a potential approach for advanced wound care applications because of their superior biocompatibility, moisture-retentive characteristics and regenerative ability [18]. Cellulose, produced from natural sources, including plants or bacteria, is a multi-functional substrate owing to its biodegradability, lack of toxicity, and structural resemblance to the extracellular matrix [19]. When augmented with a hydrogel system, anion exchange cellulose-based wound dressings can absorb redundant wound exudates and simultaneously provide a moist microenvironment to promote wound cell migration and proliferation [20]. Moreover, the porous architecture of hydrogel-impregnated cellulose leads to gas permeability, preventing the formation of an anaerobic microbial infection [21]. Researchers have also further improved these dressings by introducing bioactive agents, including antimicrobial nanoparticles or growth factors, to promote healing and prevent infection. The ability of hydrogelbased cellulose dressings to be flexible and versatile, and thus lend themselves to a broad variety of wound conditions, from chronic ulcers to burns, makes them a promising advance over current standard wound care materials.

The synthesis of hydrogel-based cellulose requires high-level procedures, based on the desirable characteristics of cellulose and hydrogel networks. Typically, the process begins with the extraction or production of cellulose, which can be derived from plant sources [22], or regenerated cellulose like cellulose acetate [23] and cellulose abietate [24]. Crosslinking is an important process in hydrogel synthesis, which can usually be performed by using chemical crosslinkers such as glutaraldehyde [26-28], citric acid [28-29], and genipin [30-31] to assemble a stable three-dimensional network.

Physical crosslinking techniques, such as freeze-thaw cycles or UV irradiation, are used in parallel to avoid the existence of toxic residue. Generally, the hydrogel is swollen with water, yielding a highly hydrated structure resembling the extracellular matrix. Other functionalities can be added by embedding bioactive molecules into the fabrication process [23]. This technology guarantees the biocompatibility, flexibility, and suitability of hydrogel-based cellulose dressings for different wound-care purposes.

Recent advances in natural product-based therapeutics have highlighted the potential of plant-derived extracts as effective antibacterial agents. One such promising candidate is the peel extract of white dragon fruit (*Hylocereus undatus*), which contains a rich profile of phenolics, flavonoids, and betacyanins known for their antimicrobial, antioxidant, and anti-inflammatory properties. Previous studies have reported the antibacterial efficacy of white dragon fruit peel extract against common wound pathogens, including *Staphylococcus aureus* and *Escherichia coli*, making it a valuable natural additive for wound care applications [32-33].

Current wound dressings often rely on synthetic materials that lack biodegradability and antibacterial function, limiting their effectiveness in promoting optimal healing. Although cellulose-based hydrogels offer a promising biocompatible alternative, the influence of different crosslinkers and the use of biomass-derived nanocellulose remain underexplored for wound dressing applications. In this study, a hydrogel based on nanocellulose will be made with two types of cross-linking agents, namely citric acid (CA) and epichlorohydrin (ECH). Nanocellulose isolated from pine flowers and then hydrolyzed with formic acid has been reported in previous studies by Zakiyya et al. [22]. Pine wood is one of the major forestry commodities in Indonesia, widely utilized across various sectors such as construction, furniture, and the paper industries. As a result, large amounts of pine wood waste are generated, making it a readily available and sustainable source of cellulose for value-added applications like hydrogel synthesis. Additional characterization of nanocellulose was carried out with PSA and TEM. The hydrogel produced was characterized by FTIR and SEM, as well as additional tests, namely the release test, swelling test, and antibacterial test.

EXPERIMENTAL SECTION

Materials

The materials used in this study include: pine flowers obtained from the pine forest in Batu, Indonesia, White dragon fruit skin powder (*H. undatus*) from Materia Medica, Batu, Indonesia, HCl (Smart-Lab), NH₄OH (Smart-Lab), NaOH (Merck), NaOCl, aquadest, formic acid (Smart-Lab), CA (Smart-Lab), ECH (Sigma-Aldrich), urea (Merck), ethanol, nutrient agar, *S. aureus* (ATCC 25923) and *E. coli*. (ATCC 25922) The equipments used in this study include glassware, rotary evaporator (IKA), analytical balance (Ohaus), ultrasonic (Delta D150H 48 kHz), universal pH paper (Macherey-Nagel), grinder, magnetic stirrer (Corning PC620O), and oven (Memmert).

Instrumentation

The instruments used in this study include: Fourier-transform infrared spectroscopy (FTIR, Shimadzu 8400s), X-ray diffractometer (XRD, PANalytical Xpert-Pro), transmission electron microscope (TEM, JEOL JEM 1400), scanning electron microscope (SEM, Hitachi FlexSEM 1000), UV-visible spectrophotometer (Shimadzu UV-1601), and particle size analyzer (PSA, Zetasizer Nano Series).

Procedure

Nanocellulose production

Nanocellulose was isolated from pine flowers. The isolation process and characterization results of nanocellulose have been reported in Zakiyya et al. [22]. Furthermore, nanocellulose with the smallest crystallinity index and size was selected for the hydrogel material, namely nanocellulose from hydrolysis using 60% CA and 1 h reaction time.

Hydrogel fabrication

Making nanocellulose hydrogels is done by adding 10 mL of solution containing NaOH/urea/aquadest with a mass ratio of 6:4:90 (w/w). Then, nanocellulose was

added to the solution. The solution is stirred at 600 rpm for 30 min and cooled at $-12\,^{\circ}\text{C}$ for 15 h. The concentration of hydrogel constituents is shown in detail in Table 1. The solution obtained is left at room temperature and stirred at 600 rpm for 30 min. The solution is added with cross-linker and stirred at 600 rpm for 30 min at room temperature. The mixture was observed to thicken after the addition of the crosslinker, indicating ongoing crosslinking. Then the mixture is poured and dried at 50 °C for 19 h.

Characterization

TEM analysis. Nanocellulose was analyzed for morphology, size distribution, and diffraction patterns using TEM. TEM analysis in this study was carried out using image mode to determine the shape and size of nanoparticles. The analysis stages were initially prepared with carbon plates as sample media. Next, the powdered sample was first dispersed using ethanol. Then the carbon plate was dipped into the sample and air-dried. After drying, the carbon plate was inserted into the sample tube and the image was taken [34].

Swelling test. The swelling test stages refer to the method of Khaleghi et al. [35] with modification. The hydrogel was weighed first before the swelling test. Then the hydrogel was soaked in distilled water at room temperature for 24 h. Then the hydrogel was removed from the soaking and weighed. The swelling percentage was measured using Eq. (1);

Table 1. Concentration of hydrogel constituents

Sample code	Citric acid	ECH
	(g)	(mL)
H-CA 2	2.0	0.0
H-CA 3	3.0	0.0
H-CA 4	4.0	0.0
H-ECH 2	0.0	2.0
H-ECH 3	0.0	3.0
H-ECH 4	0.0	4.0

Note: H-CA 2 = hydrogel citric acid 2%, H-CA 3 = hydrogel citric acid 3%, H-CA 4 = hydrogel citric acid 4%, H-ECH 2 = hydrogel epichlorohydrin 2%, H-ECH 3 = hydrogel epichlorohydrin 3%, H-ECH 4 = hydrogel epichlorohydrin 4%. All materials are produced using 6.0 g NaOH, 4.0 g urea, 90.0 mL aquadest, 0.3 g nanocellulose, and 0.3 g white dragon fruit peel extract.

$$SR\% = \frac{m_t - m_0}{m_0} \times 100\% \tag{1}$$

while, m_0 is the mass of the hydrogel before swelling and m_t is the mass of the hydrogel after swelling.

FTIR study. A total of 5 mg of cellulose sample was mixed with 95 mg of KBr homogeneously. Then the mixture was ground and made into KBr pellets with an S/N ratio of 20000:1, to form a thin plate. The plate was placed on the slit, and a beam of light was passed through it to form an FTIR spectrum at 400–4000 cm⁻¹ [36].

SEM analysis. Analysis using SEM aims to determine the morphology of the hydrogel surface. SEM imaging is carried out by cutting the dried hydrogel sample into small pieces and mounting it on a specimen holder.

Antibacterial test

Antibacterial activity test was conducted using the disc method. The test bacteria used were *S. aureus* (Gram positive) and *E. coli* (Gram negative). Bacterial cultures were streaked on the surface of nutrient agar and autoclaved at 121 °C for 20 min. The hydrogel was molded into a circle with a diameter of 6 mm and placed on the medium. The test medium was incubated at 37 °C for 24 h. Measurement of antibacterial activity was carried out by measuring the diameter of the clear zone produced in the test medium. The bacterial inhibition zone was measured using Eq. (2) [37].

Inhib. zone = inhib. zone diameter – hydrogel plate diameter (2)

Release test

The release test was used to measure the amount of white dragon fruit peel extract released from the hydrogel. The hydrogel was soaked in distilled water and the white dragon fruit peel extract released at 2, 4, 6, 8, 10, 12, 14, and 24 h UV-vis was measured using spectrophotometer. The maximum absorption wavelength (λ_{max}) was determined by measuring the absorption of a 0.005 g/10 mL white dragon fruit peel extract solution.

■ RESULTS AND DISCUSSION

Nanocellulose

Nanocellulose is produced from the cellulose hydrolysis process using the sonication method with a

dispersing solution in the form of formic acid with concentration variations of 10, 30, and 60% and time variations of 45 and 60 min. This hydrolysis results have been reported in Zakiyya et al. [22]. Furthermore, based FTIR and XRD characterization nanocellulose from 60% formic acid 60 min hydrolysis was selected as a material for making hydrogel because the product has a smaller crystallinity index and crystal size than others. The smallest crystallinity index indicates that the product has a larger amorphous area. Hydrogels formed from cellulose with amorphous areas have better elasticity [38]. The smallest particle size was chosen because hydrogels formed from small-sized nanocellulose have a homogeneous and smooth physical appearance [39]. The selected nanocellulose was further characterized by TEM.

TEM Characterization

TEM was used to examine the shape of cellulose nanofibers produced by hydrolysis with 60% w/v formic acid, followed by ultrasonically for 1 h, as illustrated in Fig. 1. A dense network of entangled nanofibers with widths primarily in the nanometer range can be seen in the images, demonstrating that the cellulose microstructure has been successfully broken down into nanoscale dimensions. The average fiber diameter is between 10 and 30 nm (calculated using ImageJ software), which is in line with the usual measurements for cellulose nanofibers made by acid hydrolysis.

Darker patches indicate localized agglomerations or thicker concentrations of cellulose, while numerous light-contrasting regions throughout the image indicate thin, translucent fibrillar structures. Both individual and bundled fibers indicate partial fibrillation, in which some bigger fiber aggregates are still present. This could be because of post-sonication re-agglomeration or insufficient defibrillation. The cleavage of amorphous regions in the cellulose matrix, which facilitated the release of crystalline nanofibers, was probably aided by the hydrolysis with formic acid. Furthermore, it seems that 1 h of ultrasonication is enough to encourage additional dispersion and fiber size reduction, while some residual bundling is still visible. Because of the

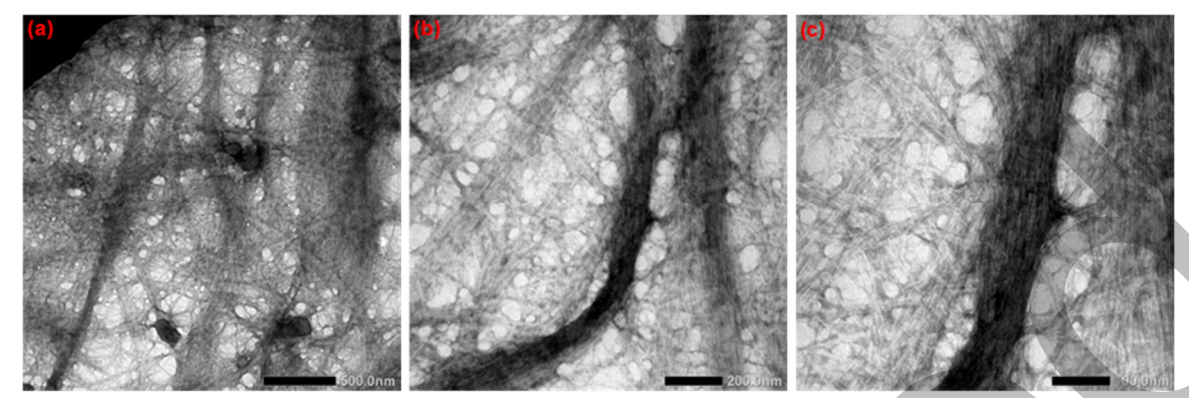


Fig 1. TEM diffraction pattern of nanocellulose with (a) 30k×, (b) 75k×, and (c) 150k× magnifications

interfibrillar entanglements that may maintain mechanical integrity, the observed networked structure also raises the possibility of film-forming uses. Similar research also shows that the hydrolysis of cellulose with CA can reduce fiber size [40-41].

Hydrogel Fabrication

Hydrogels are hydrophilic polymers in the form of a three-dimensional viscoelastic network containing water which is many times the dry weight and swell up in the physiological media. The mechanical bondage and chemical cross-linking of hydrogels can serve to provide structural and physical stability [42]. The nanocellulose used as the starting material in making this hydrogel is 60% ultrasonicated formic acid because it has the smallest crystallinity index value and particle size [22]. The size of 60% ultrasonicated formic acid nanocellulose is included in the range of colloidal dispersed particle sizes. In this study, the hydrogel formed a colloidal system as a gel colloid with a solid dispersed phase (nanocellulose) and a liquid dispersing medium (water).

Fig. 2(a–d) shows the hydrogel after the washing process with distilled water. The texture produced by the hydrogel with ECH cross-linker is more flexible than the hydrogel with CA cross-linker. Guo et al. [43] stated that making a hydrogel using cellulose/ECH produced clear and transparent hydrogel The schematic representation of hydrogel formation can be shown in Fig. 3(a). The hydroxyl group of nanocellulose becomes an alcoholate anion. Then this alcoholate anion attacks the epoxy group of ECH to form monoether chloropropanediol. The Cl atom undergoes cleavage, and there is a nucleophilic

attack from the alcoholate anion of the other nanocellulose chain so that cross-linking occurs between ECH and nanocellulose [44]. The reaction mechanism of hydrogel using CA cross-linker through the formation of an intermolecular diester is explained in Fig. 3(b). CA, when heated, will release water molecules and form cyclic anhydride. The formation of ester bonds occurs between the cyclic anhydride and hydroxyl group of nanocellulose. After the first esterification stage, the formation of the second cyclic anhydride occurs through heating. Then esterification occurs between the second cyclic anhydride of CA and hydroxyl group of nanocellulose [45].

Swelling Index Result

The swelling test is used to determine the ability of hydrogel to absorb water. The swelling mechanism is the diffusion of water into the pores of the hydrogel. The swelling index value of the hydrogel with ECH crosslinker is higher than that of the hydrogel with CA crosslinker (Table 3). This indicates that the water absorption capacity of the hydrogel with ECH cross-linker is greater than that of CA. The swelling index of hydrogels with ECH cross-linkers increases with the increasing concentration of ECH. This is because the increasing concentration of ECH will cause an increase in hydrogel cross-linking, so that the hydrogel structure network formed will be greater [46]. As a result, the ability to absorb water is also higher. Meanwhile, the swelling index of hydrogels with CA cross-linkers is inversely proportional to the CA concentration. The higher the concentration of CA, the lower the swelling index value.

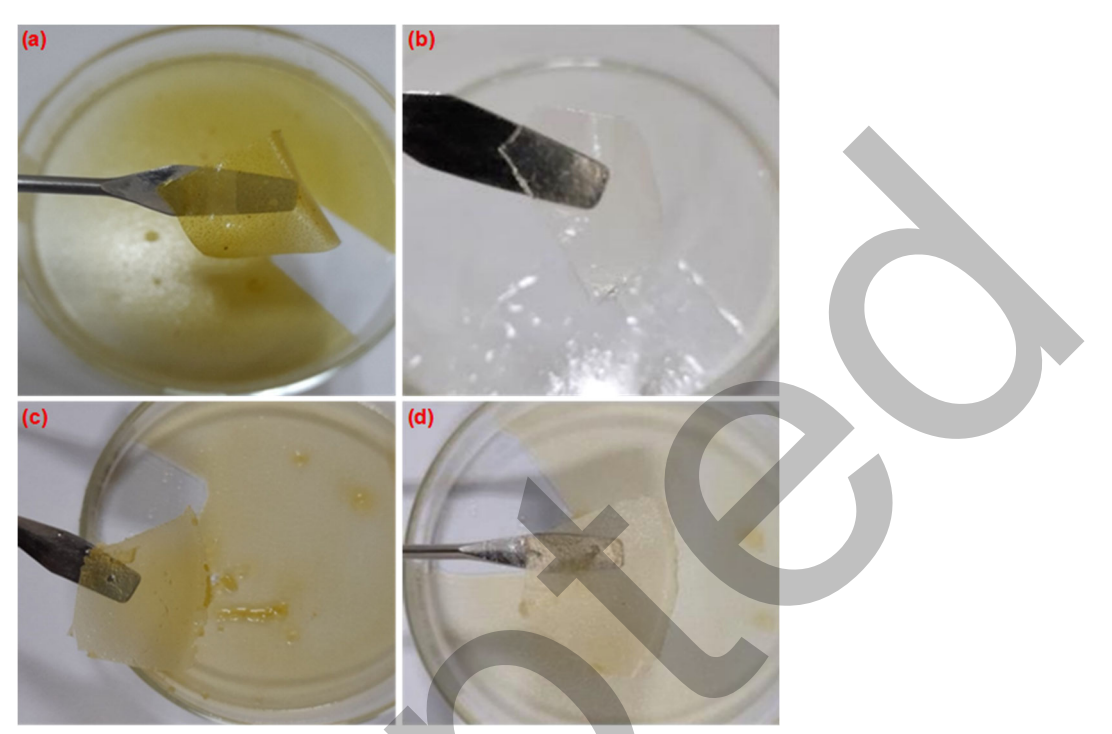
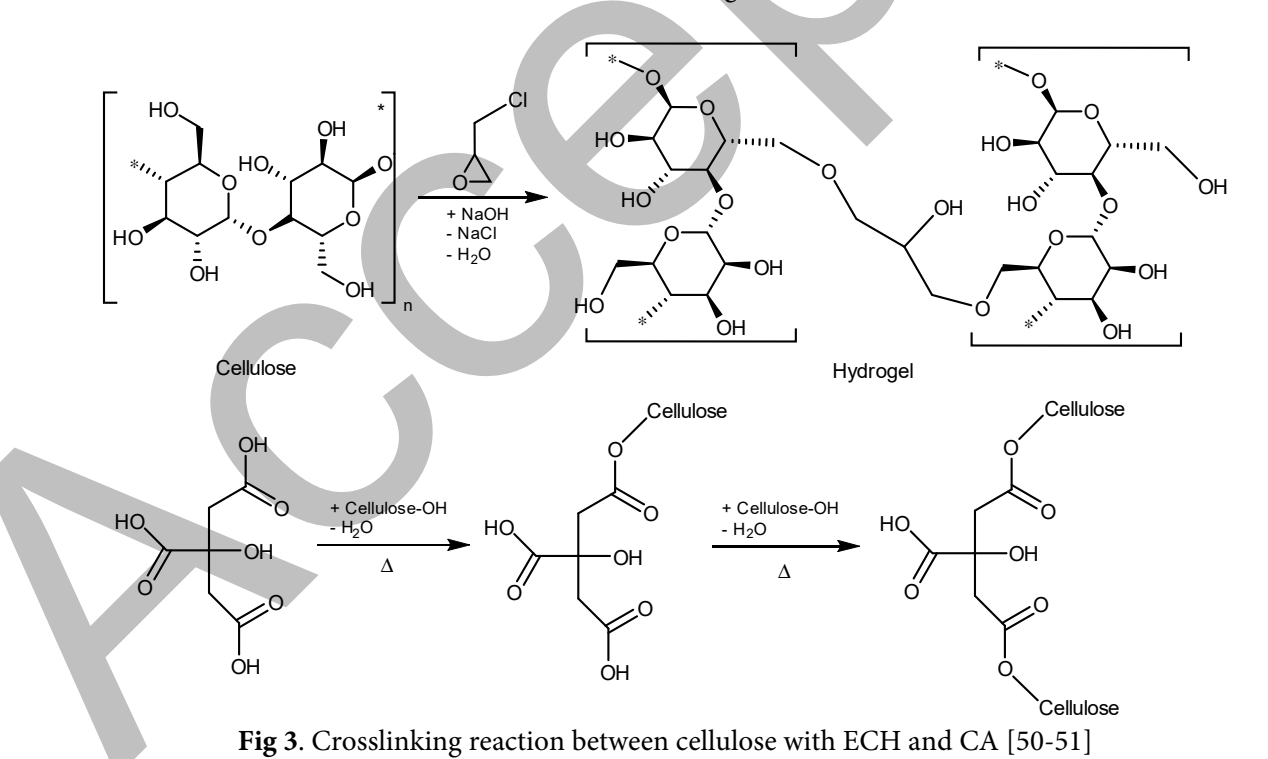


Fig 2. Hydrogel with 3% ECH linker (a) with and (b) without the addition of white dragon fruit extract. Hydrogel with 3% CA linker (c) with and (d) without the addition of white dragon fruit extract



The higher the concentration of CA, the higher the density of hydrogel cross-linking. So, this causes the swelling ability to be low.

Hydrogels crosslinked with ECH and CA exhibit significant differences in their physical and chemical properties (Table 4). Hydrogels crosslinked with ECH

Table 3. Swelling index of hydrogel

	0 1 0
Hydrogel type	Swelling index (%)
H-CA 2%	42.27
H-CA 3%	32.59
H-CA 4%	22.96
H-ECH 2%	54.50
H-ECH 3%	92.02
H-ECH 4%	111.57

possess larger pore sizes, higher thermal stability, greater mechanical strength, and a higher swelling index compared to those crosslinked with CA. Increasing the concentration of ECH leads to a more expanded hydrogel network, thereby enhancing its water absorption capacity. In contrast, hydrogels crosslinked with CA form a denser network structure with smaller pore sizes, resulting in a decreased swelling index as the CA concentration increases due to the higher crosslinking density. This behavior is closely related to the swelling mechanism, where water diffuses into the pores of the hydrogel; a looser network structure, as seen in ECH-crosslinked hydrogels, facilitates greater water diffusion, whereas a denser structure, as observed in CA-crosslinked hydrogels, restricts water uptake and reduces swelling capacity (Fig. 4(a-d)).

Antibacterial Test Result

This antibacterial test was conducted using the disc diffusion method. The bacteria used were *S. aureus* and *E. coli*. Table 5 shows the diameter of the inhibition zone of the hydrogel with and without white dragon fruit peel extract. The white dragon fruit peel extract on hydrogel improved the activity. CA hydrogel 4% and ECH hydrogel 4% could not inhibit *S. aureus* bacteria. Meanwhile, the addition of extract has a larger inhibition zone against *S. aureus* bacteria than the ECH hydrogel. The diameter

value is above 5.07 ± 0.020 mm. However, in *E. coli* bacteria, no activity is recorded. *E. coli* has a lipid bilayer membrane, namely lipopolysaccharides composed of phospholipid chains on the outer membrane and peptidoglycan on the inner membrane. The outer membrane functions as a selectively permeable membrane and protects bacteria from harmful substances. While *S. aureus* only has one membrane, namely peptidoglycan. This is what causes *E. coli* to be more resistant than *S. aureus* [50].

Hydrogels can inhibit *S. aureus*. The active compounds in crude white dragon fruit peel extract are trapped in the hydrogel network during the gelling process. When the hydrogel containing white dragon fruit peel extract comes into direct contact with the agar media that has been spread with bacteria, the active compounds will be released. So that the active

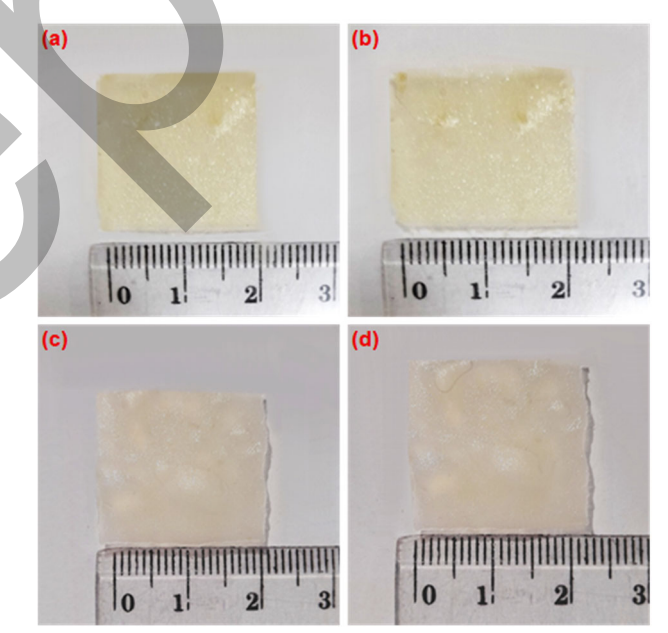


Fig 4. Hydrogel ECH 3%: (a) before and (b) after swelling; and CA 3%: (c) before and (d) after swelling

Table 4. Differences between crosslinked hydrogels with ECH and CA

Property	ECH-crosslinked hydrogels	CA-crosslinked hydrogels	Literature
Viscosity	Data not specified	Increase with CA concentration	[47]
Surface area	Larger pores (~46 μm)	Nanoporous structure with smaller pores	[47-48]
Thermal stability	Higher (> 300 °C)	Decrease with more CA	[47-48]
Crystallinity	Data not specified	Decrease with CA crosslinking	[48]
Mechanical strength	Higher strength	Lower strength, higher flexibility	[48-49]
Swelling behavior	Higher swelling ratio	Decrease with more CA, high at optimal CA levels	[48]

Table 5. Inhibition zone diameter of the hydrogel

Cample	Inhibition zone diameter (mm)	
Sample	S. aureus	E. coli
White dragon fruit skin extract	5.07 ± 0.020	0.00
H-CA4	0.00	0.00
H-CA2 + extract	6.10 ± 0.020	0.00
H-CA3 + extract	5.81 ± 0.020	0.00
H-CA4 + extract	5.51 ± 0.007	0.00
H-ECH4	0.00	0.00
H-ECH2 + extract	6.13 ± 0.007	0.00
H-ECH3 + extract	6.15 ± 0.000	0.00
H-ECH4 + extract	6.30 ± 0.007	0.00

Note: H-CA2 = hydrogel citric acid 2%, H-CA3 = hydrogel citric acid 3%, H-C4 = hydrogel citric acid 4%, H-ECH2 = hydrogel epichlorohydrin 2%, H-ECH3 = hydrogel epichlorohydrin 3%, H-ECH4 = hydrogel epichlorohydrin 4%, and extract = from white dragon fruit

compounds in the crude white dragon fruit peel extract will penetrate the cell walls of *S. aureus* bacteria, as a result, the integrity and permeability of the membrane are damaged; the cells undergo lysis and an inhibition zone is formed [51]. The concentration of ECH hydrogel release is directly proportional to the concentration of ECH cross-linker. This is in line with the trend of inhibition zone values in the antibacterial test. The higher the concentration of ECH, the more hydrogel networks are formed, so that more extract is absorbed. As a result, when the hydrogel comes into direct contact with the test medium containing bacteria, the amount of extract released is also higher.

FTIR Result

FTIR analysis was used to determine the presence or absence of white dragon fruit peel extract in the hydrogel. Fig. 5 shows the FTIR spectra of the extract and hydrogel. The *H. undatus* peel extract has band absorption at 3420, 2924, 1600–1712, 1054–1200 cm⁻¹, indicating the stretching vibration of phenolic or alcohol groups (O–H), aliphatic C–H, C=O of ester, aldehyde, or carboxylic acid, and C–OH stretching alcohol or carboxylic acid. ECH and CA hydrogels without extract showed a decrease in O–H and C=O bands compared to the extract. In H-ECH4, the C–O–C band appeared more clearly, which is typical of ECH, indicating that the

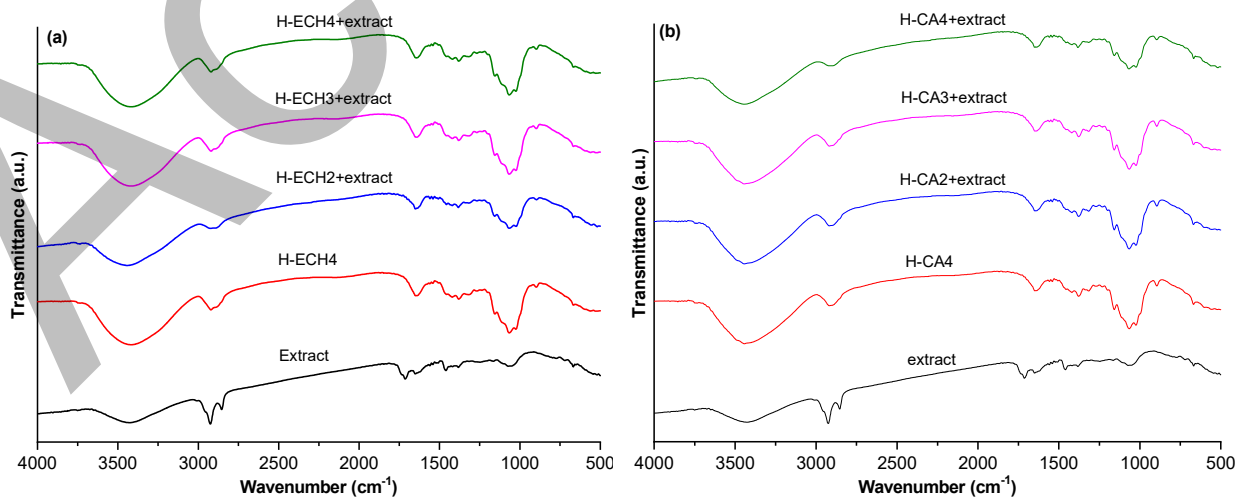


Fig 5. FTIR spectra of white dragon fruit peel extract and hydrogel prepared using (a) ECH and (b) CA crosslinker

hydrogel network structure was formed through crosslinking [51]. While H-CA4 showed an increase in the 1720 cm⁻¹ band, namely ester, indicating the formation of crosslinking [28]. The addition of white dragon fruit peel extract resulted in an increase in the intensity of O-H (~3300 cm⁻¹), which originated from the phenolics. New functional groups were not identified, indicating no new chemical reactions between the hydrogel and the extract. In addition, there was a small shift and change in the intensity of the O-H and C=O peaks, indicating physical interactions, especially hydrogen bonds between the extract and the hydrogel network. Both ECH and CAbased hydrogels were able to interact with the extract through physical mechanisms, i.e., hydrogen bonds, without forming new covalent bonds. The type of crosslinker affects the structure of the hydrogel: ECH forms a more stable ether bond, while CA forms an ester bond that allows for environmental response. This difference is important in drug or active compound release applications, where CA-based systems may be more suitable for controlled release due to the biodegradable nature of esters.

Release Test Result

The measurement value of λ_{max} of white dragon fruit peel extract is 251 nm [52]. The effect of cross-linker concentration on release ability is shown in Fig. 6. Hydrogels using ECH and CA cross-linkers show that release ability is directly proportional to swelling ability. Fig. 6(a) shows the release ability of hydrogel with CA cross-linker of white dragon fruit peel extract. In the first 2 h, the release ability of CA hydrogel at all cross-linker concentrations occurred very quickly. This is due to the high difference in concentration between the hydrogel

containing white dragon fruit peel extract and the outer solution, which causes the extract to diffuse from the hydrogel to the outer solution [53]. Hydrogel CA 2 and 3% had constant release ability after 6 h. While the release ability of the hydrogel CA 4% was constant after 10 h. This indicates that hydrogel CA 2% and 3% were more constant than hydrogel CA 4%. The concentration of white dragon fruit peel extract released in hydrogel CA 2%> hydrogel CA 3%> hydrogel CA 4%.

The graph in Fig. 6(b) shows the release concentration of white dragon fruit peel extract on hydrogel with crosslinker ECH. In the first 2 h, the release ability of ECH hydrogel at all concentrations occurred very quickly. After that, the release rate was slower until it reached a constant time. The release concentration of hydrogel ECH2 and 3% was constant after 10 h. While the release concentration of hydrogel ECH 4% was constant after 8 h. This indicates that hydrogel ECH 4% is more constant than hydrogel ECH 3% and 2%.

SEM Morphology

SEM analysis was used to determine the morphology of the hydrogel using an ECH cross-linker agent. H-ECH was chosen because it has better properties in terms of inhibiting antibacterial and swelling ability than H-CA. Fig. 7 shown the morphology of hydrogels ECH cross-linkers without (Fig. 7(a)) and with extract (Fig. 7(b)) has a smooth surface. In the study of Zhao et al. [54] it was stated that the synthesis of hydroxyethyl cellulose/soy protein film using ECH produced a smooth structure. The surface of the hydrogel that does not contain extracts appears smoother and more homogeneous. This structure indicates that the polymer network formation process is

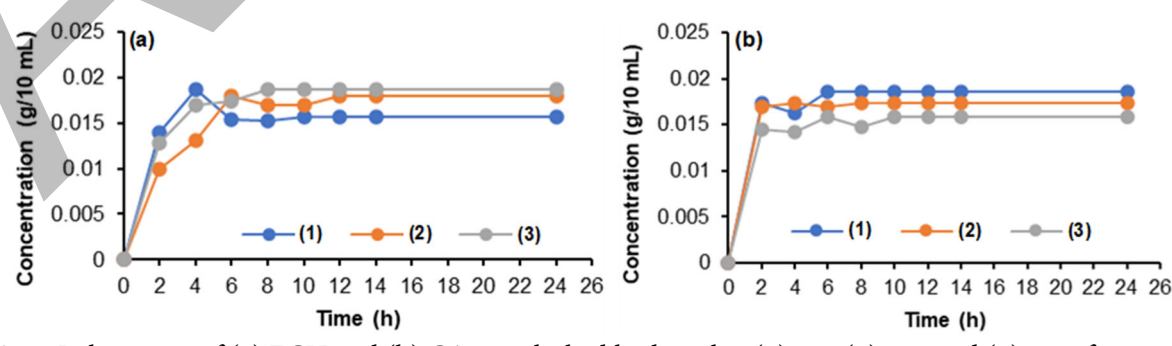


Fig 6. Release test of (a) ECH and (b) CA crosslinked hydrogel at (1) 2%, (2) 3%, and (3) 4% of concentration

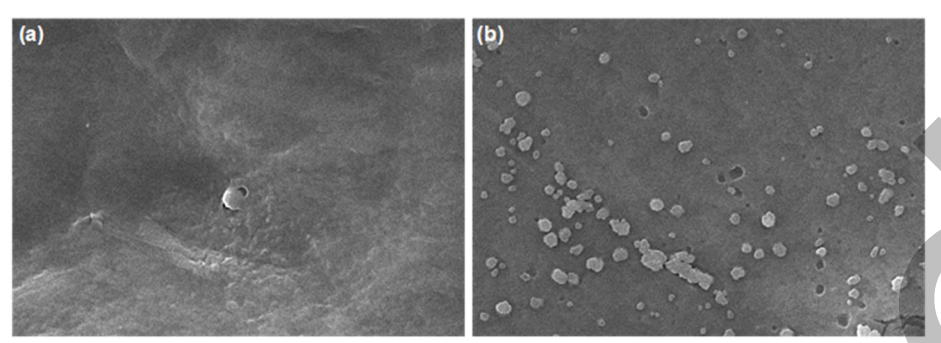


Fig 7. Surface morphology of (a) H-ECH and (b) H-ECH3 at 10k× magnifications

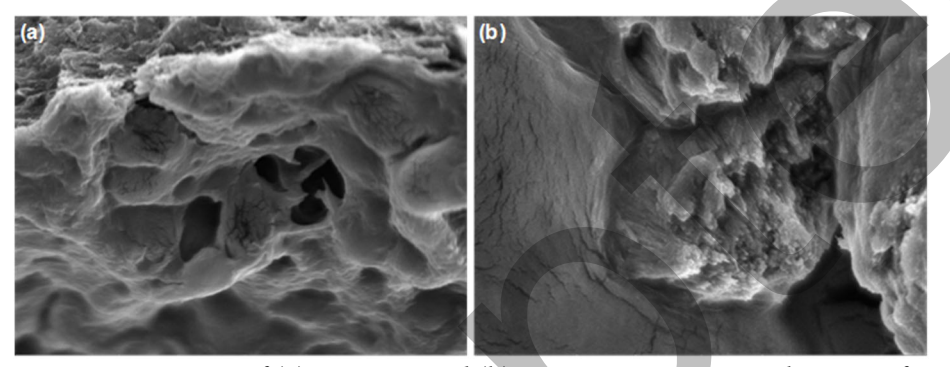


Fig 8. SEM cross-section of (a) H-ECH3 and (b) H-ECH3+extract at 10k× magnifications

taking place well and evenly, without any interference from foreign materials. This reflects the regularity in the formation of crosslinking between the polymer and the crosslinker. In contrast, the surface of the hydrogel added with the extract showed a rougher, inhomogeneous texture and had small protrusions or pores. This morphology indicates that the extract is likely to be unevenly dispersed in the hydrogel matrix.

The morphology of ECH hydrogel observed through SEM cross-section (through side section) is shown in Fig. 8(a–b). The SEM image of the cross-section shows that the hydrogel without extract has a more hollow structure than the hydrogel with extract. The larger and clearer cavities in the hydrogel without extract reflect the polymer network formed with loose interchain spaces. In contrast, the addition of extract causes the structure to become denser and more compact. This is due to compounds in the extract, such as polyphenols and flavonoids, which can fill the cavities and form bonds with the polymer chains, thereby reducing porosity and strengthening the hydrogel network [55].

CONCLUSION

Cellulose-based hydrogels crosslinked with CA and ECH displayed a good prospect for the development of high-performance wound dressing. The FTIR analysis supported the successful crosslinking and the detection of characteristic functional groups of both crosslinkers. SEM imaging showed a porous morphology, necessary for moisture retention, gas transport, and drug storage. The swelling tests showed that hydrogels crosslinked with ECH exhibited higher water absorption capacity compared to CA-crosslinked hydrogels, making them more suitable for wounds with heavy exudate. Analysis of drug release found a controlled and sustained release profile, especially in CA crosslinked hydrogels, as a result of increased swelling characteristics. Antibacterial assay also validated further use of both hydrogels, with CA-crosslinked hydrogels with extract (H-CA + extract) demonstrating slightly enhanced inhibitory effects on prevalent wound pathogens. This improvement is attributed to the presence of white dragon fruit peel extract, which has been previously reported to possess antibacterial activity. These results provide the nature of the versatility of cellulose-based hydrogels and the great role of crosslink agents on their physical, chemical, and biological performances, which can offer very useful information about the design of the optimal wound dressing materials.

ACKNOWLEDGMENTS

The author acknowledges that this research is part of a project funded by the PDUPT research grant from Brawijaya University under contract number 00140.12/UN10.A0501/B/PT.01.03.2/2024.

■ CONFLICT OF INTEREST

The authors declare that there is no conflict of interest regarding the publication of this article.

AUTHOR CONTRIBUTIONS

All authors have equal contribution to the manuscript. Masruri did conceptualization, supervision, and reviewing; Urfa 'Uyunin Zakiyya did data collection; Nur Ikhtiarini did data compilation and draft; Muchammad Zainul Anwar adding the data and analysis.

REFERENCES

- [1] Rodgers, K., and Jadhav, S.S., 2018, The application of mesenchymal stem cells to treat thermal and radiation burns, *Adv. Drug Delivery Rev.*, 123, 75–81.
- [2] Holmes, S.P., Rivera, S., Hooper, P.B., Slaven, J.E., and Que, S.K.T., 2022, Hydrocolloid dressing versus conventional wound care after dermatologic surgery, *JAAD Int.*, 6, 37–42.
- [3] Le, L.T.T., Giang, N.N., Chien, P.N., Trinh, X.T., Long, N.V., Anh, L.T.V., Nga, P.T., Zhang, X.R., Nam, S.Y., and Heo, C.Y., 2023, Enhancement of wound healing efficacy by chitosan-based hydrocolloid on Sprague Dawley rats, *In Vivo*, 37 (3), 1052–1064.
- [4] Nguyen, N., Dulai, A.S., Adnan, S., Khan, Z., and Sivamani, R.K., 2025, Narrative review of the use of hydrocolloids in dermatology: Applications and benefits, *J. Clin. Med.*, 14 (4), 1345.
- [5] Zhang, W., Liu, L., Cheng, H., Zhu, J., Li, X., Ye, S., and Li, X., 2024, Hydrogel-based dressings designed

- to facilitate wound healing, *Mater. Adv.*, 5 (4), 1364–1394.
- [6] Chelu, M., Calderon Moreno, J.M., Musuc, A.M., and Popa, M., 2024, Natural regenerative hydrogels for wound healing, *Gels*, 10 (9), 547.
- [7] Gounden, V., and Singh, M., 2024, Hydrogels and wound healing: Current and future prospects, *Gels*, 10 (1), 43.
- [8] Jokar, F., Rahaiee, S., Zare, M., Nasiri Kenari, M., and Mirzakhani, N., 2023, Bioactive wound dressing using bacterial cellulose/dextran biopolymers loaded with pomegranate peel extract: Preparation, characterization and biological properties, *J. Drug Delivery Sci. Technol.*, 84, 104461.
- [9] Polverino, G., Russo, F., and D'Andrea, F., 2024, Bioactive dressing: A new algorithm in wound healing, *J. Clin. Med.*, 13 (9), 2488.
- [10] Vivcharenko, V., and Przekora, A., 2021, Modifications of wound dressings with bioactive agents to achieve improved pro-healing properties, *Appl. Sci.*, 11 (9), 4114.
- [11] Ikhtiarini, N., Kamil, M.Z., Bukit, B.F., Juliadmi, D., Prasetiyo, K.W., Fransiska, D., Sedayu, B.B., Subiyanto, B., Sulastiningsih, I.M., Rochima, E., Arivendan, A., and Syamani, F.A., 2025, Biocompatible composites based on alginate, polycaprolactone, and nanocellulose: A review, *Int. J. Biol. Macromol.*, 311 (Pt. 1), 143423.
- [12] Tudoroiu, E.E., Dinu-Pîrvu, C.E., Albu Kaya, M.G., Popa, L., Anuţa, V., Prisada, R.M., and Ghica, M.V., 2021, An overview of cellulose derivatives-based dressings for wound-healing management, *Pharmaceuticals*, 14 (12), 1215.
- [13] Afzali, M., Esfandiaribayat, N., and Boateng, J., 2025, Medicated and multifunctional composite alginate-collagen-hyaluronate based scaffolds prepared using two different crosslinking approaches show potential for healing of chronic wounds, *Drug Delivery Transl. Res.*, 15 (7), 2483–2508.
- [14] Liang, W., Ni, N., Huang, Y., and Lin, C., 2023, An advanced review: Polyurethane-related dressings for skin wound repair, *Polymers*, 15 (21), 4301.

- [15] Niculescu, A.G., and Grumezescu, A.M., 2022, An up-to-date review of biomaterials application in wound management, *Polymers*, 14 (3), 421.
- [16] Paneer Selvam, S., Ayyappan, S., I Jamir, S., Sellappan, L.K., and Manoharan, S., 2024, Recent advancements of hydroxyapatite and polyethylene glycol (PEG) composites for tissue engineering applications A comprehensive review, *Eur. Polym. J.*, 215, 113226.
- [17] Yang, W., Zhu, Y., He, Y., Xiao, L., Xu, P., Puglia, D., and Ma, P., 2022, Preparation of toughened poly(lactic acid)-poly(ε-caprolactone)-lignin nanocomposites with good heat- and UV-resistance, *Ind. Crops Prod.*, 183, 114965.
- [18] Partovi, A., Khedrinia, M., Arjmand, S., and Ranaei Siadat, S.O., 2024, Electrospun nanofibrous wound dressings with enhanced efficiency through carbon quantum dots and citrate incorporation, *Sci. Rep.*, 14 (1), 19256.
- [19] Yu, P., Wei, L., Yang, Z., Liu, X., Ma, H., Zhao, J., Liu, L., Wang, L., Chen, R., and Cheng, Y., 2024, Hydrogel wound dressings accelerating healing process of wounds in movable parts, *Int. J. Mol. Sci.*, 25 (12), 6610.
- [20] Hodge, J.G., Zamierowski, D.S., Robinson, J.L., and Mellott, A.J., 2022, Evaluating polymeric biomaterials to improve next generation wound dressing design, *Biomater. Res.*, 26 (1), 50.
- [21] de Carvalho, R.S.F., Mahnke, L.C., Palácio, S.B., Barbosa, W.T., Hodel, K.V.S., Barbosa, J.D.V., Melo, F.A.D., Chorilli, M., Meneguin, A.B., Pinto, F.C.M., de Morais, M.A., and Aguiar, J.L.A., 2025, Bacterial cellulose hydrogel produced by *Gluconacetobacter hansenii* using sugarcane molasses as medium: Physicochemical characterization for wound healing applications, *Carbohydr. Polym. Technol. Appl.*, 9, 100632.
- [22] Zakiyya, U., 'Uyunin, U., Masruri, M., Ningsih, Z., and Srihardyastutie, A., 2020, Sonication-assisted pine cone flower cellulose hydrolysis using formic acid, *IOP Conf. Ser.: Mater. Sci. Eng.*, 833 (1), 012001.
- [23] Cindradewi, A.W., Bandi, R., Park, C.W., Park, J.S., Lee, E.A., Kim, J.K., Kwon, G.J., Han, S.Y., and Lee, S.H., 2021, Preparation and characterization of

- cellulose acetate film reinforced with cellulose nanofibril, *Polymers*, 13 (17), 2990.
- [24] Ikhtiarini, N., Masruri, M., Ulfa, S.M., Rollando, R., and Widodo, N., 2024, Antibacterial activity of hydrogels produced from nanocellulose derivatives for controlled drug delivery, *Trop. J. Nat. Prod. Res.*, 8 (5), 7068–7072.
- [25] Akakuru, O.U., and Isiuku, B.O., 2017, Chitosan hydrogels and their glutaraldehyde-crosslinked counterparts as potential drug release and tissue engineering systems Synthesis, characterization, swelling kinetics and mechanism, *J. Phys. Chem. Biophys.*, 7 (6), 256.
- [26] Distantina, S., Rochmadi, R., Fahrurrozi, M., and Wiratni, W., 2013, Preparation and characterization of glutaraldehyde-crosslinked kappa carrageenan hydrogel, *Eng. J.*, 17 (3), 57–66.
- [27] Musa, B.H., and Hameed, N.J., 2021, Effect of Effect of crosslinking agent (glutaraldehyde) on the mechanical properties of (PVA/starch) blend and (PVA/PEG) binary blend films, *J. Phys.: Conf. Ser.*, 1795 (1), 012064.
- [28] Mali, K.K., Ghorpade, V.S., Dias, R.J., and Dhawale, S.C., 2023, Synthesis and characterization of citric acid crosslinked carboxymethyl tamarind gumpolyvinyl alcohol hydrogel films, *Int. J. Biol. Macromol.*, 236, 123969.
- [29] Poudel, R., Dutta, N., and Karak, N., 2023, A mechanically robust biodegradable bioplastic of citric acid modified plasticized yam starch with anthocyanin as a fish spoilage auto-detecting smart film, *Int. J. Biol. Macromol.*, 242 (Pt. 2), 125020.
- [30] Xu, D., Hui, Y.Y., Zhang, W., Zhao, M.N., Gao, K., Tao, Xing-R., and Wang, J.W., 2024, Genipin-crosslinked hydrogels for food and biomedical applications: A scientometric review, *Int. J. Biol. Macromol.*, 282, 137478.
- [31] Wang, L., Ding, X., He, X., Tian, N., Ding, P., Guo, W., Okoro, O.V., Sun, Y., Jiang, G., Liu, Z., Shavandi, A., and Nie, L., 2024, Fabrication and properties of hydrogel dressings based on genipin crosslinked chondroitin sulfate and chitosan, *Polymers*, 16 (20), 2876.

- [32] Hendra, R., Masdeatresa, L., Abdulah, R., and Haryani, Y., 2019, Antibacterial activity of red dragon peel (*Hylocereus polyrhizus*) pigment, *J. Phys.: Conf. Ser.*, 1351 (1), 012042.
- [33] Nur, M.A., Uddin, M.R., Meghla, N.S., Uddin, M.J., and Amin, M.Z., 2023, *In vitro* anti-oxidant, anti-inflammatory, anti-bacterial, and cytotoxic effects of extracted colorants from two species of dragon fruit (*Hylocereus* spp.), *Food Chem. Adv.*, 2, 100318.
- [34] Zanoni, I., Keller, J.G., Sauer, U.G., Müller, P., Ma-Hock, L., Jensen, K.A., Costa, A.L., and Wohlleben, W., 2022, Dissolution rate of nanomaterials determined by ions and particle size under lysosomal conditions: Contributions to standardization of simulant fluids and analytical methods, *Chem. Res. Toxicol.*, 35 (6), 963–980.
- [35] Khaleghi, M., Ahmadi, E., Khodabandeh Shahraki, M., Aliakbari, F., and Morshedi, D., 2020, Temperature-dependent formulation of a hydrogel based on hyaluronic acid–polydimethylsiloxane for biomedical applications, *Heliyon*, 6 (3), e03494.
- [36] Kowalczuk, D., and Pitucha, M., 2019, Application of FTIR method for the assessment of immobilization of active substances in the matrix of biomedical materials, *Materials*, 12 (18), 2972.
- [37] Hossain, M.R., Biplob, A.I., Sharif, S.R., Bhuiya, A.M., and Sayem, A.S.M., 2023, Antibacterial activity of green synthesized silver nanoparticles of *Lablab purpureus* flowers extract against human pathogenic bacteria, *Trop. J. Nat. Prod. Res.*, 7 (8), 3647–3651.
- [38] Nicu, R., Ciolacu, F., and Ciolacu, D.E., 2021, Advanced functional materials based on nanocellulose for pharmaceutical/medical applications, *Pharmaceutics*, 13 (8), 1125.
- [39] de Lima, G.G., Ferreira, B.D., Matos, M., Pereira, B.L., Nugent, M.J.D., Hansel, F.A., and Magalhães, W.L.E., 2020, Effect of cellulose size-concentration on the structure of polyvinyl alcohol hydrogels, *Carbohydr. Polym.*, 245, 116612.
- [40] Li, B., Xu, C., Kronlund, D., Määttänen, A., Liu, J., Smått, J.H., Peltonen, J., Willför, S., Mu, X., and Xu, W.Y., 2015, Cellulose nanocrystals prepared via formic acid hydrolysis followed by TEMPO-

- mediated oxidation, *Carbohydr. Polym.*, 133, 605–612.
- [41] Sun, Y., Lin, L., Pang, C., Deng, H., Peng, H., Li, J., He, B., and Liu, S., 2007, Hydrolysis of cotton fiber cellulose in formic acid, *Energy Fuels*, 21 (4), 2386–2389.
- [42] Jacob, S., Nair, A.B., Shah, J., Sreeharsha, N., Gupta, S., and Shinu, P., 2021, Emerging role of hydrogels in drug delivery systems, tissue engineering and wound management, *Pharmaceutics*, 13 (3), 357.
- [43] Guo, B., Chen, W., and Yan, L., 2013, Preparation of flexible, highly transparent, cross-linked cellulose thin film with high mechanical strength and low coefficient of thermal expansion, ACS Sustainable Chem. Eng., 1 (11), 1474–1479.
- [44] Udoetok, I.A., Dimmick, R.M., Wilson, L.D., and Headley, J.V., 2016, Adsorption properties of cross-linked cellulose-epichlorohydrin polymers in aqueous solution, *Carbohydr. Polym.*, 136, 329–340.
- [45] Ismail, H., Irani, M., and Ahmad, Z., 2013, Starch-based hydrogels: Present status and applications, *Int. J. Polym. Mater. Polym. Biomater.*, 62 (7), 411–420.
- [46] Islam, T., Danishuddin, D., Tamanna, N.T., Matin, M.N., Barai, H.R., and Haque, M.A., 2024, Resistance mechanisms of plant pathogenic fungi to fungicide, environmental impacts of fungicides, and sustainable solutions, *Plants*, 13 (19), 2737.
- [47] Lacaran, J.V.T., Narceda, R.J., Bilo, J.A.V., and Leaño Jr., J.L., 2021, Citric acid crosslinked nanofibrillated cellulose from banana (*Musa acuminata* × *balbisiana*) pseudostem for adsorption of Pb²⁺ and Cu²⁺ in aqueous solutions, *Cellul. Chem. Technol.*, 55 (3-4), 403–415.
- [48] Muharam, S., Yuningsih, L.M., and Sumitra, M.R., 2017, Characterization of superabsorbent hydrogel based on epichlorohydrin crosslink and carboxymethyl functionalization of cassava starch, *AIP Conf. Proc.*, 1862 (1), 030083.
- [49] Sharmin, N., Rosnes, J.T., Prabhu, L., Böcker, U., and Sivertsvik, M., 2022, Effect of citric acid crosslinking on the mechanical, rheological and barrier properties of chitosan, *Molecules*, 27 (16), 5118.

- [50] Mota, L.O., and Gimenez, I.F., 2023, Cellulose-based materials crosslinked with epichlorohydrin: A mini review, *Rev. Virtual Quim.*, 15 (1), 159–170.
- [51] Dharmalingam, K., and Anandalakshmi, R., 2019, Fabrication, characterization and drug loading efficiency of citric acid crosslinked NaCMC-HPMC hydrogel films for wound healing drug delivery applications, *Int. J. Biol. Macromol.*, 134, 815–829.
- [52] Nasution, H., Harahap, H., Dalimuthe, N.F., Ginting, M.H.S., Jaafar, M., Tan, O.O.H., Aruan, H.K., and Herfananda, A.L., 2022, Hydrogel and effects of crosslinking agent on cellulose-based hydrogels: A review, *Gels*, 8 (9), 568.
- [53] Keirudin, A.A., Zainuddin, N., and Yusof, N.A., 2020, Crosslinked carboxymethyl sago starch/citric acid hydrogel for sorption of Pb²⁺, Cu²⁺, Ni²⁺ and Zn²⁺

- from aqueous solution, *Polymers*, 12 (11), 2465.
- [54] Zhao, Y., He, M., Zhao, L., Wang, S., Li, Y., Gan, L., Li, M., Xu, L., Chang, P.R., Anderson, D.P., and Chen, Y., 2016, Epichlorohydrin-cross-linked hydroxyethyl cellulose/soy protein isolate composite films as biocompatible and biodegradable implants for tissue engineering, *ACS Appl. Mater. Interfaces*, 8 (4), 2781–2795.
- [55] Alzaben, F., Fat'hi, S., Elbehiry, A., Alsugair, M., Marzouk, E., Abalkhail, A., Almuzaini, A.M., Rawway, M., Ibrahem, M., Sindi, W., Alshehri, T., and Hamada, M., 2022, Laboratory diagnostic methods and antibiotic resistance patterns of *Staphylococcus aureus* and *Escherichia coli* strains: An evolving human health challenge, *Diagnostics*, 12 (11), 2645.